Available online at www.sciencedirect.com
ScienceDirect
Ceramics International 37 (2011) 2747–2753
CERAMICS INTERNATIONAL
www.elsevier.com/locate/ceramint

Giant dielectric response and mixed-valent structure in the layered-ordered double-perovskite ceramics

W.Z. Yang [a], M.S. Fu [b], X.Q. Liu [a,*], H.Y. Zhu [a], X.M. Chen [a]

[a] Department of Materials Science and Engineering, Laboratory of Dielectric Materials, Zhejiang University, 38 Zheda Road, Hangzhou 310027, China
[b] School of Materials Science and Engineering, Shanxi Materials Analysis and Research Center, Northwestern Polytechnical University, Xi'an 710072, China

Received 22 February 2011; received in revised form 15 April 2011; accepted 15 April 2011
Available online 22 April 2011

Abstract

Origin of giant dielectric response in the layered-ordered double-perovskite La_2CuSnO_6 ceramics was investigated in the present work. Apart from the main layered-ordered double-perovskite La_2CuSnO_6 phase, minor $La_2Sn_2O_7$ secondary phase was detected. There were two dielectric relaxations in the curve of temperature dependence of dielectric properties of La_2CuSnO_6 ceramics. Both of dielectric relaxations were thermal activated process. The low temperature relaxation should be attributed to the mixed-valent structure (Cu^{2+}/Cu^{3+}) since the activation energy was similar to that of La_2CuTiO_6 ceramics. While the high temperature relaxation was closely related to the thermal activated hopping process of electrical conduction. After annealing the sample in N_2 and O_2 atmosphere, the trend of dielectric behaviors and ac conductivities were the same at high temperature. This result confirmed that the high temperature relaxation was closely related to the electrical conduction.

Keywords: B. X-ray method; C. Dielectric properties; D. Perovskites; Mixed-valent structure

1. Introduction

The study of transition-metal perovskites is of great interest due to the abundant magnetic and electrical properties in these kinds of materials. Substitutions of the B site with two different ions B′ and B″ in the ABO_3 compound result in the complex perovskite structure $A(B',B'')O_3$, the physical properties of which depend on the oxidation state and the ordering degree of B′ and B″ [1,2]. Cation ordering in complex perovskite oxides with two or more cations mixed in the octahedrally coordinated B-sites, is an interesting phenomenon and has been extensively studied, and is known to have strong influence on the structural and physical properties (magnetic, electric, dielectric, ferroelectric, piezoelectric, etc.) of these materials [3].

Double-perovskite is an important kind of complex perovskite, and three kinds of double-perovskite have been discovered, i.e., disordered, rock salt ordered and layered ordered perovksite [1]. Among these double-perovskites, La_2CuSnO_6 is the unique layered-ordered one that consists of three kinds of 2D layers, CuO_2, SnO_2, and LaO layers. The ideal size of the CuO_2 layer is between those of the SnO_2 and the LaO layer because Sn^{4+} has a larger ionic radius than Cu^{2+} and the LaO layer has the rock salt configuration. The mismatching is compromised by tilting, rather than elastic deformation of the CuO_6 and SnO_6 octahedra. Magnetic susceptibility measurements from 5 to 300 K show weak ferromagnetism [4,5]. Since La^{3+} and Sn^{4+} are both non-magnetic, this behavior directly demonstrates the antiferromagnetic nature of the CuO_2 lattice accompanied by a spin-canted weak ferromagnetism, as reported before [6]. The saturation magnetization measured on cooling to 5 K corresponds to a ferromagnetic moment of 6.4×10^{-3} μ_B/Cu [4]. Earlier studies mainly focused on the atomic Cu/Sn B-site ordering, electronic structure and magnetic properties of La_2CuSnO_6 materials [4,5,7,8].

Recently, the giant dielectric constant and the mixed-valent structure have been discovered in double-perovskite La_2CuTiO_6 ceramic [9], which has a disorder distribution of Cu and Ti among the B sites in the structure. The giant dielectric response is attributed to the mixed-valent structure (Cu^{+}/Cu^{2+} and Ti^{3+}/Ti^{4+}). As shown in the previous work [3], the order of B sites will significantly affect the dielectric properties of materials

* Corresponding author. Tel.: +86 571 87951410; fax: +86 571 87951410.
E-mail address: xqliu@zju.edu.cn (X.Q. Liu).

0272-8842/$36.00
doi:10.1016/j.ceramint.2011.04.029

with double-perovksite structure, so the study of dielectric properties of layered-ordered double-perovskite La_2CuSnO_6 ceramic is nontrivial. So far, the dielectric properties of layered-ordered double-perovskite La_2CuSnO_6 ceramic have not been investigated to our knowledge.

In the present work, La_2CuSnO_6 ceramics are prepared by solid-state sintering process, and dielectric properties are investigated in a broad frequency and temperature range.

2. Experimental procedure

La_2CuSnO_6 powders were synthesized by a solid-state reaction process using the starting materials of La_2O_3 (99.99%), CuO (99%) and SnO_2 (99.5%), which were weighted and mixed by ball milling with ZrO_2 balls in ethanol for 24 h, then dried and calcined at 1050 °C in air for 3 h to yield the desired materials. The calcined powders were ball milled for 24 h and then dried. The dried powders with 7 wt% polyvinyl alcohol (PVA) were pressed into pellets, and then sintered in air at 1175 °C for 3 h. Some La_2CuSnO_6 samples were annealed at 975 °C for 6 h in a flow of O_2 or N_2. Crystal data were carried out by powder X-ray diffraction (XRD) using Cu Kα radiation (Rigaku D/max 2550 PC, Rigaku Co., Tokyo, Japan) in the 2θ range of 10–130° at a step width of 0.02° with dwelling time of 1.5 s for each step. Structure refinement was performed by the Rietveld method using the Fullprof package [10,11]. The samples for TEM analysis were prepared by disaggregating the ceramic, followed by grinding in an agate mortar. The powders were then suspended in ethanol and dispersed onto standard amorphous carbon-coated copper TEM microgrids. The selected area electron diffraction (SAED) patterns and high-resolution lattice images were obtained at 200 kV by high-resolution transmission electron microscopy (HRTEM, JEM-2010, JEOL Ltd, Tokyo, Japan). X-ray photoemission spectroscopy (XPS) experiments were carried out on a RBD upgraded PHI-5000 C ESCA system (Perkin Elmer, Waltham, MA) with Mg Kα radiation (hν=1253.6 eV) or Al Kα radiation (hν=1486.6 eV). The experimental curve was fitted with a program (XPSPEAK4.1) that made use of a combination of Gaussian–Lorentzian lines. The dielectric characteristics and ac conductivities of these ceramics were evaluated with a broadband dielectric spectrometer (Turnkey Concept 50, Novocontrol Technologies, Hundsangen, Germany) in a broad range of temperature (133–573 K) and frequency (1 Hz–10 MHz) with a heating rate of 2 K/min, and the silver paste was adopted as electrodes.

3. Results and discussion

Fig. 1 shows the Rietveld analysis results of the XRD patterns for as-sintered La_2CuSnO_6 ceramics at room temperature. Apart from the main La_2CuSnO_6 phase, a minor amount (2.40(3) wt%) of secondary phase, $La_2Sn_2O_7$, is existed in the present ceramics. The space group of the main La_2CuSnO_6 phase is $P\ 2_1/m(11)$, and the cell parameters are $a = 8.4987(2)$ Å, $b = 7.8155(2)$ Å, $c = 7.8160(2)$ Å, and $\beta = 91.0932(9)°$, respectively. The Rietveld analyses are also done on the N_2-annealed and O_2-annealed samples to find out the possibility of structural differences between these samples. The experimental parameters for Rietveld refinement of as-sintered, N_2-annealed and O_2-annealed La_2CuSnO_6 ceramics are given in Table 1. From the table, one can find the differences of cell parameters are all within experimental error, and this indicates the crystalline structure does not change after annealed in nitrogen and oxygen. The content of secondary phase is almost the same in the as-sintered and O_2-annealed samples, while that of the N_2-annealed sample is a bit higher. The amount of secondary phase is very low, and the phase should not have effect on the electrical properties of the sample.

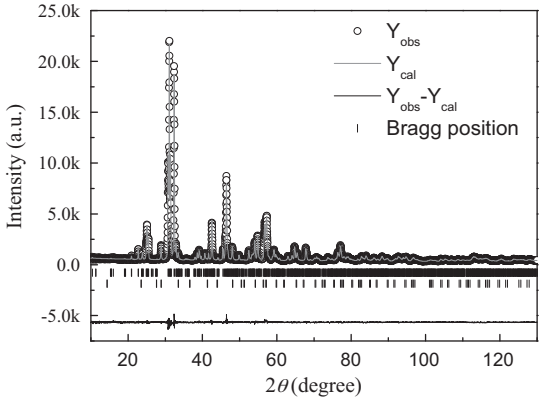

Fig. 1. Rietveld analysis results of XRD patterns for La_2CuSnO_6 ceramics: experimental, calculated and difference. Space group: $P\ 2_1/m(11)$; crystal structure: monoclinic with $a = 8.4987(2)$ Å, $b = 7.8155(2)$ Å, $c = 7.8160(2)$ Å; $\beta = 91.0932(9)°$. Minor amount (2.40(3) wt%) of $La_2Sn_2O_7$ (bottom bars) is detected.

Fig. 2a shows SAED patterns of as-sintered La_2CuSnO_6 ceramics viewed along the [1 1 0] series zone axes. The double splitting of high-order reflections indicates that two domains coexist [12]. As a result, the patterns are indexed based on two domains distinguished by the subscripts A and B, corresponding to [1 0 1] and [1 1 0] zone axes, respectively. High-resolution transmission electron microscopy image for La_2CuSnO_6 ceramics viewed along the [1 0 1] zone axes (see Fig. 2b). The 0.79 nm superlattice modulation shown in that area is double of the interplaner distance of the (0 2 0) plane and corresponds to the 1/2[0 2 0]* superreflection. The 0.62 nm superlattice modulation shown in that area is double of the interplaner distance of the $(2\,0\,2)$ plane and corresponds to the $1/2[2\,0\,2]^*$ superreflection. The tolerance factor of La_2CuSnO_6 ceramics is 0.925. According to Reaney et al. [13], the tilting of oxygen octahedra in the present ceramics occurs in both anti-phase and in-phase since the tolerance factor is smaller than 0.965. The $1/2[2\,2\,2]^*$ reflection results from the anti-phase tilting of the oxygen octahedra and/or 1:1 B-site cation ordering in the ceramics. The $1/2[2\,0\,2]^*$ reflection is attributed to the in-phase tilting of the oxygen octahedral. And the 1/2[0 2 0]* reflection is largely due to the layered ordering of Cu and Sn ions. All of these results were consistent with a layered ordering distribution of the two ions within the octahedral (B) sites of the perovskite structure [5].

Temperature dependence of the dielectric constant (ε') and dielectric loss ($\tan\delta$) for as-sintered La_2CuSnO_6 ceramics is

Table 1
Experimental parameters for X-ray powder diffraction of as-sintered and N_2-annealed La_2CuSnO_6 ceramics.

	As-sintered sample	N_2-annealed sample	O_2-annealed sample
Unit cell (space group $P\ 2_1/m$)	a = 8.49869(19) Å	a = 8.49947(19) Å	a = 8.49717(22)
	b = 7.81548(16) Å	b = 7.81543(16) Å	b = 7.81543(18) Å
	c = 7.81599(16) Å	c = 7.81588(16) Å	c = 7.81535(19) Å
	β = 91.0932(9)°	β = 91.0887(10)°	β = 91.0887(10)°
Cell volume	519.054(19) Å^3	519.090(19) Å^3	518.916(22) Å^3
Number of reflections	1992/2	1987/2	1992/2
Number of refined parameters	66	66	66
Half width parameters	U = 0.108(6)	U = 0.103(5)	U = 0.081(6)
	V = −0.026(5)	V = −0.033(5)	V = 0.004(6)
	W = 0.025(1)	W = 0.027(1)	W = 0.019(1)
	X = 0.0042(3)	X = 0.0044(3)	X = 0.0033(4)
Peak shape (Pseudo-Voigt), η	0.439(13)	0.444(13)	0.429(16)
Zero-point, 2θ (degree)	−0.0379(11)	−0.0191(11)	−0.0596(13)
Asymmetry parameter	P_1 = 0.068(4)	P_1 = 0.054(4)	P_1 = 0.051(5)
	P_2 = 0.0327(9)	P_2 = 0.0321(9)	P_2 = 0.0312(11)
Reliability factors	R_p = 6.33	R_p = 6.43	R_p = 6.86
	R_{wp} = 7.01	R_{wp} = 7.16	R_{wp} = 7.06
	χ^2 = 1.30	χ^2 = 1.33	χ^2 = 0.741
Abundances of impurities ($La_2Sn_2O_7$)	2.40(3) wt%	2.84(4) wt%	2.34(4) wt%

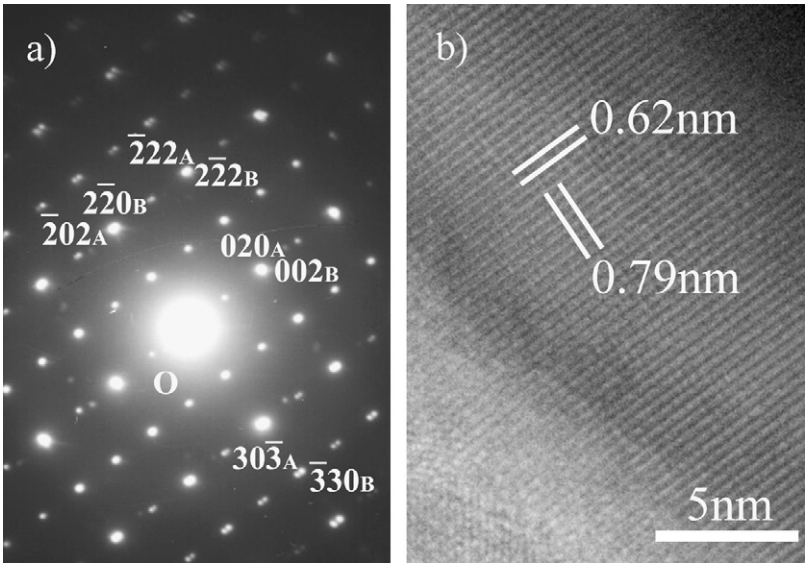

Fig. 2. (a) SAED patterns of as-sintered La_2CuSnO_6 ceramics viewed along the [1 1 0] series zone axes. (b) High-resolution transmission electron microscopy image for as-sintered La_2CuSnO_6 ceramics viewed along the [1 0 1] zone axes.

given in Fig. 3. Two dielectric relaxations are observed in the present ceramics at the temperature range of 180–300 K and 300–550 K, respectively. The dielectric constant step at low temperature is not sensitive to the applied frequency, while a giant relaxorlike dielectric stage in the high temperature range significantly suppresses with increasing frequency. The critical temperature for both dielectric relaxations increases with increasing frequency. The ε' of La_2CuSnO_6 ceramics increases with two step-like ascending stages. This is particularly noticeable in the curves measured at lower frequencies (1 kHz and 10 kHz). Two thermally activated relaxation processes are well defined in the corresponding curves of tan δ. These are typical dielectric relaxations and they are common features of giant dielectric constant materials [14–19]. To analyze the low temperature dielectric relaxation, the frequency dependence of peak temperature for the dielectric loss is plotted (see the insets in Fig. 3), and the following relationship is employed to fit the curve

$$f = f_0 \exp\left(-\frac{E_a}{k_B T_m}\right) \quad (1)$$

where E_a denotes the activation energy required for the dielectric relaxation, k_B is Boltzmann's constant, f is the applied frequency, f_0 is the pre-exponential factor and T_m is the temperature where the dielectric loss is maximum. After fitting the data with Eq. (1), the following results are obtained: the low-temperature dielectric relaxation activation energy, E_a, is 0.340 ± 0.002 eV and the value of f_0 is 1.6(1) THz. Similarly,

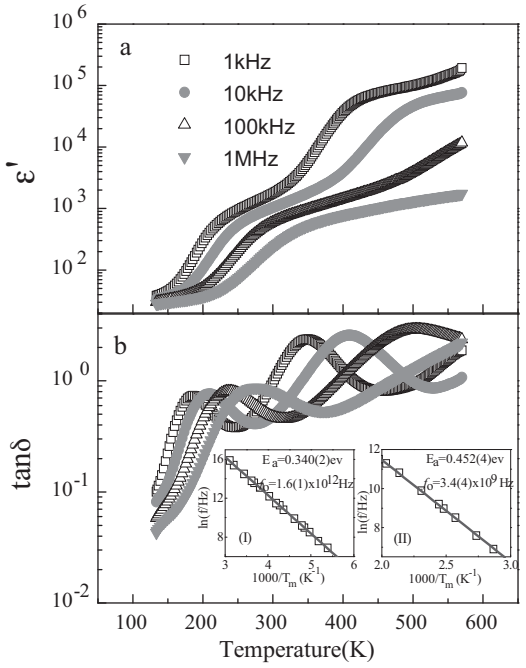

Fig. 3. Temperature dependence of dielectric properties of La_2CuSnO_6 ceramics: (a) dielectric constant, and (b) dielectric loss. The inset is the Arrhenius fitting of reciprocal peak temperature dependence of frequency at lower temperature (I) and higher temperature (II), respectively.

the fitting parameters are obtained as $E_a = 0.452 \pm 0.004$ eV and $f_0 = 3.4(4)$ GHz for high-temperature dielectric relaxation (see the insets of Fig. 3). The low temperature activation energy is very close to that of La_2CuTiO_6 (0.322 eV). The giant dielectric step in La_2CuTiO_6 is attributed to the mixed-valent structure (Cu^+/Cu^{2+} and Ti^{3+}/Ti^{4+}) [9]. The mutual feature of the low temperature dielectric relaxation in La_2CuSnO_6 and La_2CuTiO_6 leads us to deduce that the low temperature dielectric relaxation in La_2CuSnO_6 ceramics also originates from the mixed-valent structure. Fig. 4 displays the XPS spectra of Cu $2p_{3/2}$ regions of La_2CuSnO_6 ceramics. The $2p_{3/2}$ peak for Cu can be split into two peaks by Gaussian–Lorentzian curve fitting, and this shows the coexistence of Cu^{2+} and Cu^{3+} ions. The binding energies for Cu^{2+} $2p_{3/2}$ and Cu^{3+} $2p_{3/2}$ are 933.6 and 935.7 eV, respectively. Therefore, the low temperature dielectric relaxation of

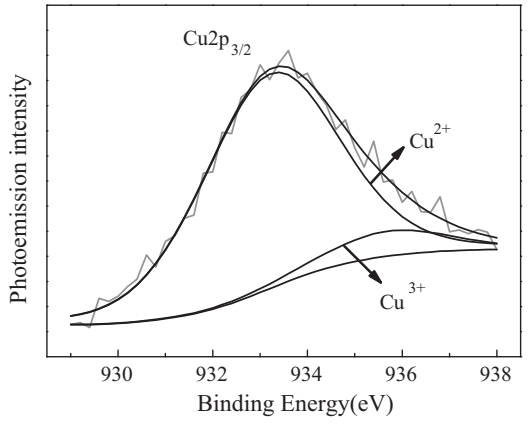

Fig. 4. XPS spectra of Cu $2p_{3/2}$ regions of La_2CuSnO_6 ceramics.

La_2CuSnO_6 ceramics should also originate from the mixed-valent structure (Cu^{2+}/Cu^{3+}), i.e. dipolar effect associated with localized charge carriers (electrons and/or polarons) hopping between spatially fluctuating lattice potentials.

To find out the origin of high temperature dielectric relaxation, the electrical conductive mechanism is considered. The bulk conductivity should be given firstly if investigation of the conductive mechanism of La_2CuSnO_6 ceramics is needed. As shown in the work of Iguchi et al. [20], the impedance spectrum is used to determine the contribution from the grain interiors, grain boundaries and interface of sample-electrode, and the response frequency decreases in the turn. The typical impedance spectra at various temperatures are shown in Fig. 5. After carefully considering the impedance data, it can be found that the equivalent circuit shown in the inset of Fig. 5 is suitable for the present spectra. The CPE is a constant phase element representing the departure from Debye-like ideality and describing the power law dependence of the impedance over several decades of frequency domain, which is commonly known as Jonscher law [21,22]. There are two obvious arcs on the plots at the temperature beyond 300 K. The high frequency arc should be ascribed to the grain interiors, and the intermediate frequency arc is the grain boundaries, while the response frequency of sample-electrode interface should be out of the measurement limit. Using the least-mean-square method, the equivalent circuit fittings are preformed and the results are shown as solid lines in the plots (see Fig. 5). The resistances of grain interiors and grain boundaries of the present ceramics at different temperatures are obtained from the above analyses, and the results are shown in Fig. 6. The resistances are plotted as the function of reciprocal temperatures, and the following Arrhenius relation is employed to fit the curve,

$$R = R_0 \exp\left(\frac{E_a}{k_B T}\right) \quad (2)$$

where R_0 is the pre-exponential term and E_a is the activation energy. The linear relationship between the bulk resistances and the reciprocal temperature is observed within the temperature range of 300–400 K. Using Eq. (2), the activation energies for grain boundaries and grain interiors are 0.369 ± 0.002 eV and 0.462 ± 0.005 eV, respectively. The activation energy of grain interiors is almost the same as that of the high temperature dielectric relaxation. This indicates the correlation between the grain interiors resistances and the high temperature dielectric relaxation.

To confirm the relationship between the high-temperature dielectric relaxation and electrical conduction, the sintered post-treatment may be a suitable way. Fig. 7 shows the frequency dependence of dielectric properties for as-sintered, N_2-annealed and O_2-annealed La_2CuSnO_6 ceramics at room temperature. The dielectric constant increases after annealing in O_2 atmosphere at lower frequencies, while it decreases sharply after annealing in N_2 atmosphere at lower frequencies. However, there is no obvious change in dielectric constant at higher frequencies. The similar trend has also been observed in the curve of dielectric loss. After annealing the sample in O_2

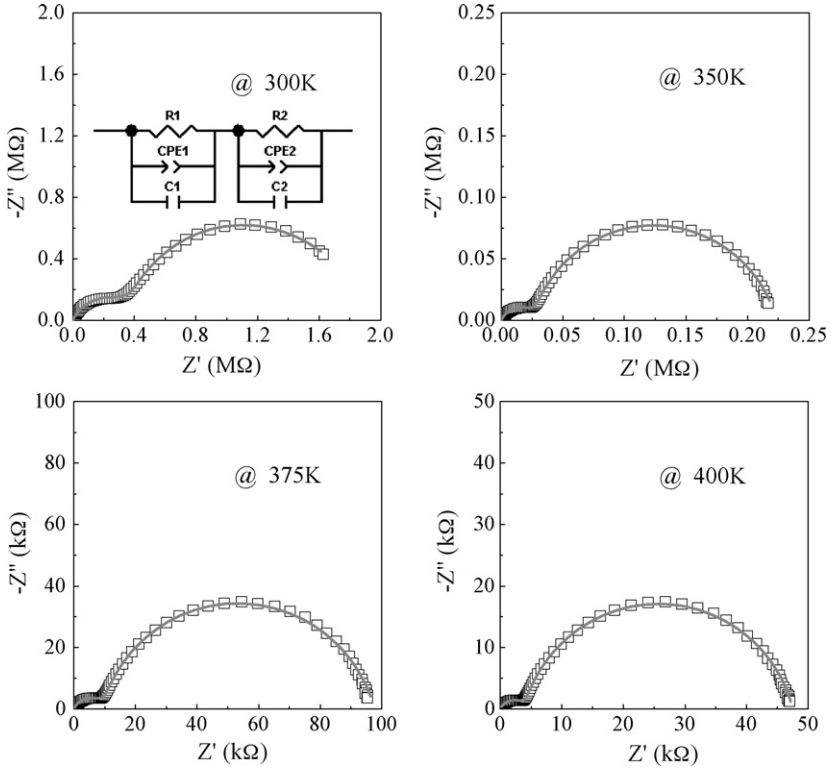

Fig. 5. Complex impedance spectra of La_2CuSnO_6 ceramics at various temperatures. The symbols are the experimental data and the solid lines are results of the fitting by equivalent circuits as shown in the inset.

and N_2 atmosphere, the dielectric loss rises up and drops down at lower frequencies, respectively. Fig. 8 presents the comparison of the dielectric behaviors and ac electrical conductivities for as-sintered samples (solid dots), N_2-annealed samples (half solid dots) and O_2-annealed samples (open dots), which shows some important information on the physical nature of the low- and high-temperature relaxations. The low-temperature dielectric relaxation is almost not changed after annealed in N_2 and O_2 atmosphere. This result confirms that the low-temperature dielectric relaxation is an intrinsic one. On the other hands, N_2-annealed and O_2-annealed treatments have a certain influence on the high-temperature dielectric relaxation, especially on the low-frequency dielectric relaxation. It is clearly seen that the dielectric constant is strongly suppressed by N_2-annealed treatment, while it is enhanced by O_2-annealed treatment at high temperature and low frequency (1 kHz). There is a slight change in dielectric constant and dielectric loss after annealing in O_2 and N_2 atmosphere at high temperature

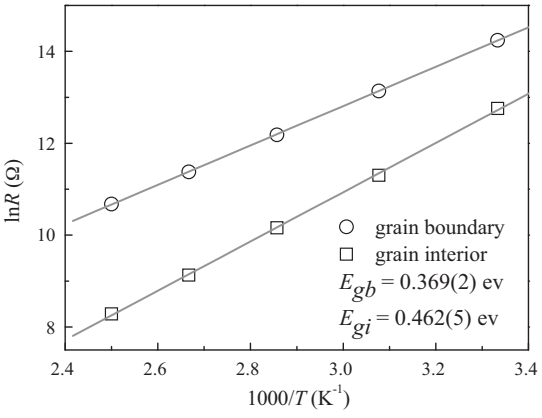

Fig. 6. Resistances of grain interiors and grain boundaries for La_2CuSnO_6 ceramics. The solid lines are results of thermally activated hopping fitting.

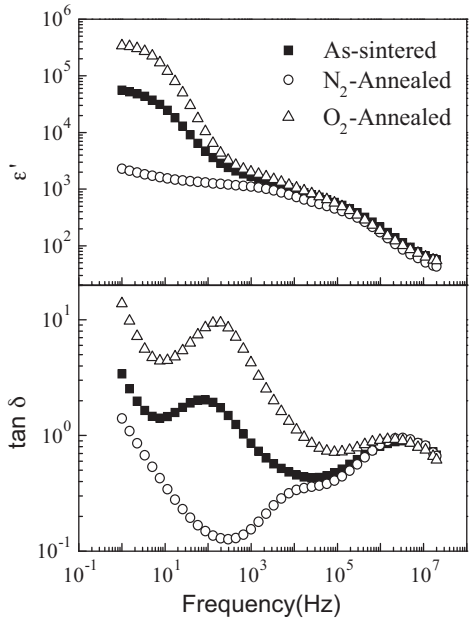

Fig. 7. Dielectric properties of as-sintered (■), N_2-annealed (○) and O_2-annealed (△) La_2CuSnO_6 ceramics at room temperature.

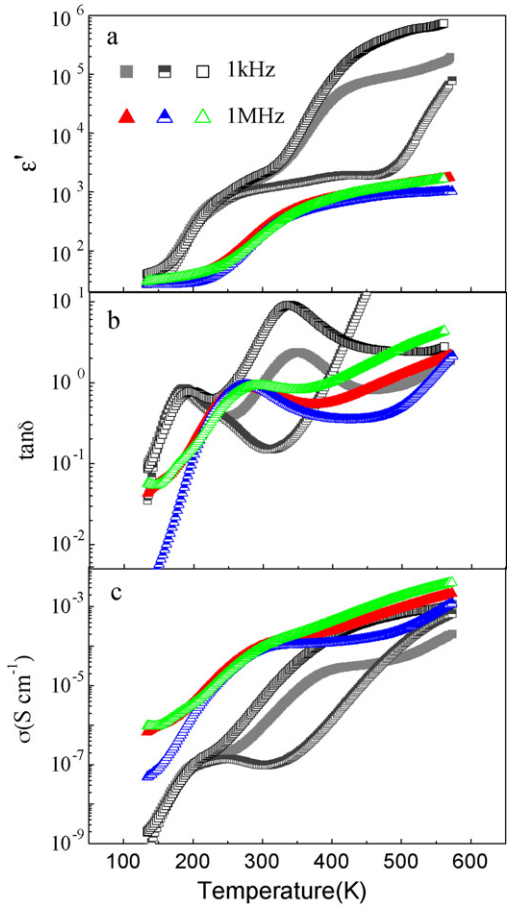

Fig. 8. (a) Dielectric constants, (b) dielectric losses and (c) ac electrical conductivities of as-sintered (solid dots), N_2-annealed (half solid dots) and O_2-annealed (open dots) La_2CuSnO_6 ceramics at the frequencies of 1 kHz and 1 MHz.

and high frequency (1 MHz). This phenomenon indicates that the low-frequency dielectric relaxation at high temperature is originated from an extrinsic mechanism, and it should be associated with the electrical conduction. Fig. 8c shows the comparison among ac electrical conductivities of as-sintered, N_2-annealed and O_2-annealed samples. The ac conductivities of N_2-annealed sample are smaller than those of the as-sintered sample, while the ac conductivities of O_2-annealed sample are larger than those of the as-sintered sample at high temperature (300–450 K) and low frequency (1 kHz). But they are almost the same at high temperature (300–450 K) and high frequency (1 MHz). The trend of dielectric behaviors and ac conductivities are nearly the same at the high temperature. This result confirms the high temperature relaxation is closely related to the electrical conduction.

Before the conclusion can be drawn, the effect of inter barrier layered capacitance (IBLC) has to be considered since the grain boundaries have much higher resistance than the grains (see Fig. 6) (Refs. [19,23]). There are only two arcs in the impendence spectra (see Fig. 5), and the arc at high frequencies is passed through the origin. This means no electrode effect is found in the considering frequency range, and the surface barrier layered capacitance (SBLC) can be excluded. There are two dielectric relaxations on the curves for the frequency dependence of dielectric constant (see Fig. 7). The low frequency dielectric relaxation should be related to the grain-boundaries barrier layered capacitance (GBLC) effect [19], and the high frequency one should be attributed to other effects, such as electrical conduction. As shown by Lunkenheimer et al. [23], the dominate mechanism giving rise to giant dielectric constants is hopping charge transport, the dielectric constant should be directly linked to the frequency by ν^{s-1} ($s < 1$). In the present ceramics, the activation energy of high temperature dielectric relaxation is almost the same as that of electrical conduction in the grain interiors, so the high-temperature dielectric relaxation should be originated from the hopping charge transport. The relationship may help explain why the dielectric constants at low frequencies are sensitive to the post-annealing, while those at high frequencies are insensitive.

4. Conclusion

Apart from the main layered-ordered double-perovskite La_2CuSnO_6 phase, minor $La_2Sn_2O_7$ secondary phase was detected. There were two dielectric relaxations in the curve of temperature dependence of dielectric properties of La_2CuSnO_6 ceramics. Both of dielectric relaxations were thermal activated process. The low temperature relaxation should be attributed to the mixed-valent structure (Cu^{2+}/Cu^{3+}) since the activation energy was similar to that of La_2CuTiO_6 ceramics. The activation energy of high temperature one was almost the same as that of electrical conductivity, and this indicated the closely correlation between the high temperature dielectric relaxation and thermal activated hopping process of electrical conduction. The ac conductivities of La_2CuSnO_6 ceramics decreased after annealing in the flow of N_2, while they increased after annealing in O_2 atmosphere at high temperature (300–450 K) and low frequency (1 kHz). But they were almost the same at high temperature (300–450 K) and high frequency (1 MHz). The trend of dielectric behaviors and ac conductivities were the same at the high temperature. This result confirmed the high temperature relaxation was closely related to the electrical conduction.

Acknowledgments

This work was supported by National Science Foundation of China under Grant Nos. 50702049, 50832005 and 51002123, Chinese National Key Project for Fundamental Researches under Grant No. 2009CB623302, and the Fundamental Research Funds for the Central Universities of China under Grand No. 2010QNA4006.

References

[1] M.T. Anderson, K.B. Greenwood, G.A. Taylor, K.R. Poeppelmeier, B-cation arrangements in double perovskites, Prog. J. Solid State Chem. 22 (1993) 197–233.
[2] Y.Q. Lin, X.M. Chen, X.Q. Liu, Relaxor-like dielectric behaviors in La_2NiMnO_6 double perovskite ceramics, Solid State Commun. 149 (2009) 784–787.

[3] S. Yañez-Vilar, M. Sánchez-Andújar, J. Rivas, M.A. Sẽnarís-Rodríguez, Influence of the cationic ordering in the dielectric properties of the La_2MnCoO_6 perovskite, J. Alloys Compd. 485 (2009) 82–87.
[4] M. Azuma, S. Kaimori, M. Takano, High-pressure synthesis and magnetic properties of layered double perovskites Ln_2CuMO_6 (Ln = La, Pr, Nd and Sm; M = Sn and Zr), Chem. Mater. 10 (1998) 3124–3130.
[5] M.T. Anderson, K.R. Poeppelmeier, La_2CuSnO_6: a new perovskite-related compound with an unusual arrangement of B cations, Chem. Mater. 3 (1991) 476–482.
[6] M.T. Anderson, K.R. Poeppelmeier, Structure-property relationships in the layered cuprate $La_{2-x}Sr_xCuSnO_6$, J. Solid State Chem. 102 (1993) 164–174.
[7] D.L. Novikov, A.J. Freeman, K.R. Poeppelmeier, V.P. Zhukov, Electronic structure of perovskite related La_2CuSnO_6, Physica C 252 (1995) 7–12.
[8] A. Masuno, M. Haruta, M. Azuma, H. Kurata, S. Isoda, M. Takano, Y. Shimakawa, Epitaxial growth and B-site cation ordering in layered double perovskite La_2CuSnO_6 thin films, Appl. Phys. Lett. 89 (2006) 211913.
[9] W.Z. Yang, M.M. Mao, X.Q. Liu, X.M. Chen, Structure and dielectric relaxation of double-perovskite La_2CuTiO_6 ceramics, J. Appl. Phys. 107 (2010) 124102.
[10] R.A. Young, The Rietveld Method, Oxford Science, New York, 1993.
[11] J. Rodriguez-Carvajal, Recent advances in magnetic structure determination by neutron powder diffraction, Phys. B 192 (1993) 55–69.
[12] W.L. Wang, H.Y. Lu, Phase-transformation-induced twinning in orthorhombic $LaGaO_3$: {1 2 1} and [0 1 0] twins, J. Am. Ceram. Soc. 89 (2006) 281–291.
[13] I.M. Reaney, E.L. Colla, N. Setter, Dielectric and structural characteristics of Ba- and Sr-based complex perovskites as a function of tolerance factor, Jpn. J. Appl. Phys. 33 (1994) 3984–3990.
[14] C.C. Homes, T. Vogt, S.M. Shapiro, S. Wakimoto, A.P. Ramirez, Optical response of high-dielectric-constant perovskite-related oxide, Science. 293 (2001) 673–676.
[15] J.B. Wu, C.W. Nan, Y.H. Lin, Y. Deng, Giant dielectric permittivity observed in Li and Ti doped NiO, Phys. Rev. Lett. 89 (2002) 217601.
[16] Z. Wang, X.M. Chen, L. Ni, X.Q. Liu, Dielectric abnormities of complex perovskite $Ba(Fe_{1/2}Nb_{1/2})O_3$ ceramics over broad temperature and frequency range, Appl. Phys. Lett. 90 (2007) 022904.
[17] X.Q. Liu, S.Y. Wu, X.M. Chen, H.Y. Zhu, Giant dielectric response in two-dimensional charge-ordered nickelate ceramics, J. Appl. Phys. 104 (2008) 054114.
[18] X.Q. Liu, Y.J. Wu, X.M. Chen, H.Y. Zhu, Temperature-stable giant dielectric response in orthorhombic samarium strontium nickelate ceramics, J. Appl. Phys. 105 (2009) 054104.
[19] S. Krohns, P. Lunkenheimer, Ch. Kant, A.V. Pronin, H.B. Brom, A.A. Nugroho, M. Diantoro, A. Loidl, Colossal dielectric constant up to gigahertz at room temperature, Appl. Phys. Lett. 94 (2009) 122903.
[20] E. Iguchi, H. Nakatsugawa, K. Futakuchi, Polaronic conduction in $La_{2-x}Sr_xCoO_4$ ($0.25 \leq x \leq 1.10$) below room temperature, J. Solid State Chem. 139 (1998) 176–184.
[21] E. Emma, McCabe, R.West Anthony, New high permittivity tetragonal tungsten bronze dielectrics $Ba_2LaMNb_4O_{15}$: M = Mn, Fe, J. Solid State Chem. 183 (2010) 624–630.
[22] O. Raymond, R. Font, N. Suárez-Almodovar, J. Portelles, J.M. Siqueiros, Frequency-temperature response of ferroelectromagnetic $Pb(Fe_{1/2}Nb_{1/2})O_3$ ceramics obtained by different precursors. Part II. Impedance spectroscopy characterization, J. Appl. Phys. 97 (2005) 084108.
[23] P. Lunkenheimer, S. Krohns, S. Riegg, S.G. Ebbinghaus, A. Reller, A. Loidl, Colossal dielectric constants in transition-metal oxides, Eur. Phys. J. Special Topics 180 (2010) 61–89.